J Mater Sci (2016) 51:1632–1643
DOI 10.1007/s10853-015-9486-y

On the sluggish recrystallization of a cold-rolled Al–Mn–Fe–Si alloy

K. Huang[1,2] · R. E. Logé[1] · K. Marthinsen[2]

Received: 16 June 2015 / Accepted: 7 October 2015 / Published online: 14 October 2015

Abstract Annealing of supersaturated AA3xxx alloys at low temperatures usually results in sluggish recrystallization kinetics. This is due to the joint effect of the following factors: low nucleation rate, reduced grain boundary mobility, and large amount of fine precipitates (dispersoids). In this paper, samples of Al–Mn–Fe–Si alloy were appropriately homogenized in different conditions to produce different microchemistries before deformation, i.e. solutes and second-phase particles. The sluggish recrystallization behaviour of these cold-rolled Al–Mn–Fe–Si samples annealed in three different conditions was then investigated, the first condition being recrystallization without precipitation, followed by recrystallization and precipitation occurring concurrently, and finally precipitation occurring before recrystallization. The results clearly show that in all these conditions, an incubation time is involved, which decreases with increasing annealing temperature and cold deformation, as well as with decreasing solute amount. Qualitative analysis of the microstructure evolution after a sudden increase of annealing temperature suggests that the effective retarding force from solute and/or particles decreases at higher temperatures. When recrystallization occurs concurrently with precipitation, the growth of successful nuclei can still be suppressed by concurrent precipitation.

✉ K. Huang
ke.huang@epfl.ch

R. E. Logé
roland.loge@epfl.ch

K. Marthinsen
knut.marthinsen@ntnu.no

[1] Thermomechanical Metallurgy Laboratory – PX Group Chair, Ecole Polytechnique Fédérale de Lausanne (EPFL), 2002 Neuchâtel, Switzerland

[2] Department of Materials Science and Engineering, Norwegian University of Science and Technology, 7491 Trondheim, Norway

Introduction

Recrystallization of single-phase materials is a complex process [1]. However, most commercial alloys contain more than one phase, and to understand the recrystallization behaviour of two-phase materials becomes often very challenging. Aluminium AA3xxx-series alloys contain Mn as their main alloying element, while other elements are often added to obtain desired mechanical properties. Since Mn has only limited solubility in Al, supersaturated Mn in solid solution after casting will precipitate as fine Mn-bearing dispersoids during subsequent thermo-mechanical processing steps [2, 3].

Slow kinetics and coarse and inhomogeneous recrystallized grain structures, commonly denoted as sluggish recrystallization behaviour, are often observed at low annealing temperatures of supersaturated AA3xxx alloys [4–8], but the actual mechanisms controlling this behaviour are far from clear. Part of the reason is that precipitated dispersoids interfere with both recovery and recrystallization, while the deformed microstructure affects both the nature and kinetics of the precipitation [1]. The fact that recrystallization and precipitation can occur in different sequences in different thermo-mechanical conditions makes the quantitative analysis even more difficult. It is well known that annealing of metallic materials at low annealing temperature leads to decreased nucleation rate and grain boundary mobility [1]. Meanwhile, fine dispersoids are usually precipitated at grain/subgrain boundaries

when annealing the deformed AA3xxx alloys at low temperatures [9], thus increasing the pinning of grain boundary migration by the Zener drag effect and suppressing nucleation of recrystallization by retarding subgrain boundary migration. All these factors jointly lead to the sluggish recrystallization at low annealing temperatures. To understand how these factors act during recrystallization is very important for tailoring the desired microstructure through appropriate thermo-mechanical processing steps, which is usually realized by numerical modelling before final trial-and-error experiments.

Despite its practical and academic importance, little systematic investigation in this area can be found in the literature [4, 6, 8, 10]. Typical recrystallization models using physically based nucleation laws usually give quantitatively reasonable predictions of the microstructures when recrystallization is not affected by precipitation [11], but they largely fail to predict the right recrystallization kinetics during annealing of dispersoid-containing materials at low temperatures [8, 12]; the prediction of recrystallized grain size is even worse. This is a clear indication that some of the key aspects during recrystallization of particle-containing materials are not well captured. The sparse models that can successfully predict the sluggish recrystallization at low temperatures invoke the introduction of an incubation time based on dislocation density [13], cell size [14], or misorientation [15] criterion. The applicability of these models should be further tested against different materials or at least the same material with different microchemistries.

It has been shown that, by varying the homogenization process of Al alloys [7, 16, 17], different microchemistry states can be obtained, i.e. solute level and second-phase particle structures, from the same starting material. It is possible to obtain tailored conditions where the sequence of recrystallization and precipitation can be manipulated, and the different physical mechanisms during the sluggish recrystallization can thus be investigated. In this paper, samples of an Al–Mn–Fe–Si alloy were firstly homogenized at different conditions to produce different microchemistries according to our previous studies [7], in terms of solutes and second-phase particles. The sluggish recrystallization behaviour of the cold-rolled Al–Mn–Fe–Si samples annealed at three different conditions was then investigated, the first condition being recrystallization without precipitation, followed by recrystallization and precipitation occurring concurrently, and finally precipitation occurring before recrystallization.

The main objective of the present work has been to analyse the sluggish recrystallization behaviour observed at different conditions for cold-deformed Al–Mn–Fe–Si alloys. The focus was on establishing a better understanding of the key aspects occurring during sluggish recrystallization, i.e. incubation time, solute drag and Zener drag. The results presented in this paper are intended to improve thermo-mechanical processing design of particle-containing materials, and shed light on strategies for numerical modelling of recrystallization affected by fine dispersoids.

Experimental procedures

Material and heat treatment

The as-received material was an AA3xxx-type direct chill (DC) casted ingot from Hydro Aluminium, Norway. The chemical composition (wt%) of the as-cast material is 0.152 % Si, 0.530 % Fe, and 0.390 % Mn with the balance of Al. More detailed information on the as-cast material can be found in Ref. [7].

From our previous investigations, the concentration level of Mn in solid solution is found to be about 0.35 wt% for the as-cast material (labelled as variant A) [7]. Since Mn only has limited solubility in Al, i.e. Mn is supersaturated in variant A, most of the Mn in solid solution will diffuse to create fine dispersoids during the following thermo-mechanical processing steps. For the purpose of comparison, some of the as-cast material (A) was subjected to a two-step homogenization treatment, the samples were first heated at 50 °C/h to 600 °C for 4 h, and then cooled at a reduced rate of 25 °C/h to 500 °C for another 4 h. The result is another variant (designated as B) with much reduced solute level of Mn and a few fine dispersoids (see Table 1), the morphology of which can be found in [18]. The main difference in terms of microchemistry between variant A and B, as shown in Table 1, is thus their different solute levels, which also means different precipitation potential. For the details on microchemistry analysis of the samples, the reader is referred to [7, 18].

These two variants were then rolled at room temperature by multiple passes to an accumulated true deformation strain of $\varepsilon = 1.6$; these samples were labelled as A1.6 and B1.6 for variant A and variant B, respectively. In addition, two samples of variant A were further deformed to a strain of $\varepsilon = 3.0$, which hereafter will be designated as A3.0. The rolling was carried out using heavily lubricated rolls and maximum roll velocity in order to obtain a microstructure similar to industrially rolled materials. The cold-rolled sheets were then heated according to different temperature–time schedules, as illustrated in Fig. 1. One set of the samples deformed to a strain of $\varepsilon = 1.6$ were annealed at low temperatures, i.e. 400 °C for A1.6 and 300 °C for B1.6 (isothermal annealing), in salt bath for 100 s, as shown in Fig. 1a. Another set of samples were subjected to a two-step annealing (Fig. 1b) where they were first annealed at

Table 1 Electrical conductivity, concentrations of solutes, average diameter, and number density of particles in the alloys studied [7]

	Electrical conductivity (m/Ωmm^2)	Concentration of Mn (wt%)	Constituent particles		Dispersoids	
			Diameter (μm)	Number density (mm^{-2})	Diameter (μm)	Number density (mm^{-2})
A	23.9	0.35	0.88	2.8×10^4	–	–
B	29.0	0.11	1.10	2.1×10^4	0.127	5.5×10^4

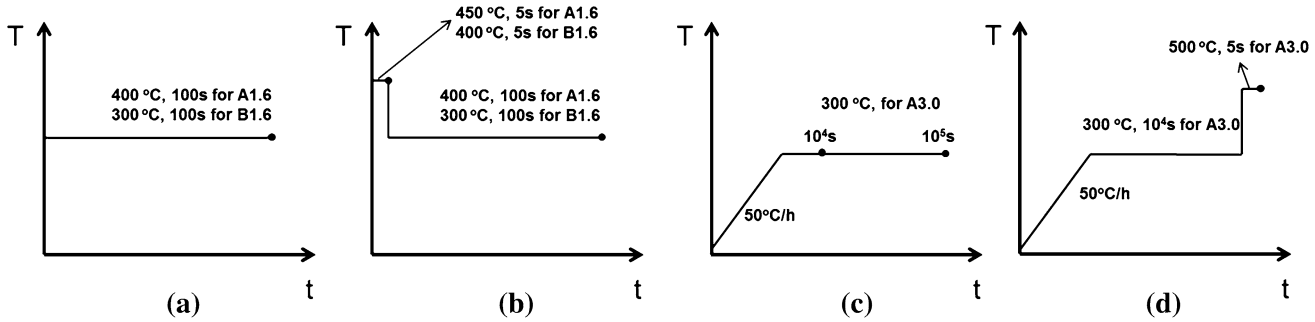

Fig. 1 Schematic graph showing the thermo-mechanical processing steps used in the current study (*black point* stands for water quench which was performed to get the microstructures in different conditions). **a** Isothermal annealing; **b** Step annealing with high temperature annealing as the first step; **c** Non-isothermal annealing; **d** Step annealing with high temperature annealing as the second step

higher temperature for 5 s, 450 °C for A1.6 and 400 °C for B1.6, and then quickly brought to the lower temperatures that are the same as in Fig. 1a. For the purpose of comparison, some of the A3.0 samples were heated at 50 °C/h to 300 °C and kept for 10^4 s (non-isothermal annealing), after which these samples were then either kept at this temperature until 10^5 s (Fig. 1c) or subjected to 5 s annealing at 500 °C (see Fig. 1d). The annealing temperature and time for the different samples in Fig. 1 is based on their recrystallization and precipitation kinetics [19, 20], and this will be further discussed below. The short time annealing step at high temperature in Fig. 1b, d is chosen to avoid significant microchemistry changes in the material. Once the samples were annealed for the desired time, they were quickly water quenched.

Microstructure characterization

The samples for electron microscopy characterization were ground and polished according to standard metallographic techniques. This was followed by electro-polishing in a solution of 30 vol% nitric acid and methanol at −30 °C and 15 V. Metallographic examinations of particles were performed using the backscattered electron (BSE) detector in a Zeiss Supra 55 field emission gun scanning electron microscope (FEG-SEM). Hardness and electrical conductivity measurements were performed on the RD–TD plane of the samples in order to follow the softening and precipitation behaviour during annealing. The average value of eight measurements at different positions of the same sample was used for each reported value, together with the standard error. Large EBSD maps of the annealed samples, with step size of 0.5–2 μm, were used to study the recrystallized grain size and recrystallized fraction, using TSL software. However, only a small part of the scanned EBSD area is presented to emphasize the newly recrystallized grains which are usually very small. For all of the micrographs presented in this paper, the horizontal direction corresponds to the rolling direction (RD), while the vertical direction is the normal direction (ND). The recrystallized grains were identified as those being partly or fully surrounded by a high-angle boundary (>15°), with a minimum grain size of 5 times the scanning step size, and with a grain orientation spread (GOS) below 0.8°. The grain size was measured as the equivalent circular diameter in the RD–ND cross section.

Results

Recrystallization and precipitation behaviour

As shown in Fig. 1, different annealing temperature–time paths were chosen to study the recrystallization and precipitation of the two different homogenization variants. The sluggish recrystallization kinetics (recrystallization

completes beyond 1000 s) was observed both when annealing the A1.6 variant at 400 °C and the B1.6 variant at 300 °C, as illustrated in Fig. 2a. For the variant A, faster recrystallization is observed at 400 °C when the cold deformation was increased to $\varepsilon = 3.0$, where recrystallization completed before 1000 s. Recrystallization accelerated for B1.6 as well when it was annealed at the higher temperature of 400 °C, where a fully recrystallized state was reached after 20 s, showing a typical S-shaped softening curve, even though the precipitation behaviour at this temperature is similar to its counterpart at 300 °C, as indicated by the evolution in electrical conductivity for the different variants in Fig. 2b. It is clear from Fig. 2b that the two variants, A1.6 and B1.6, exhibit distinctly different precipitation behaviours for the studied conditions, where A1.6 shows much stronger precipitation than B1.6 regardless of the annealing temperature and cold deformation. The precipitation for B1.6 during annealing is generally rather limited irrespective of annealing temperature.

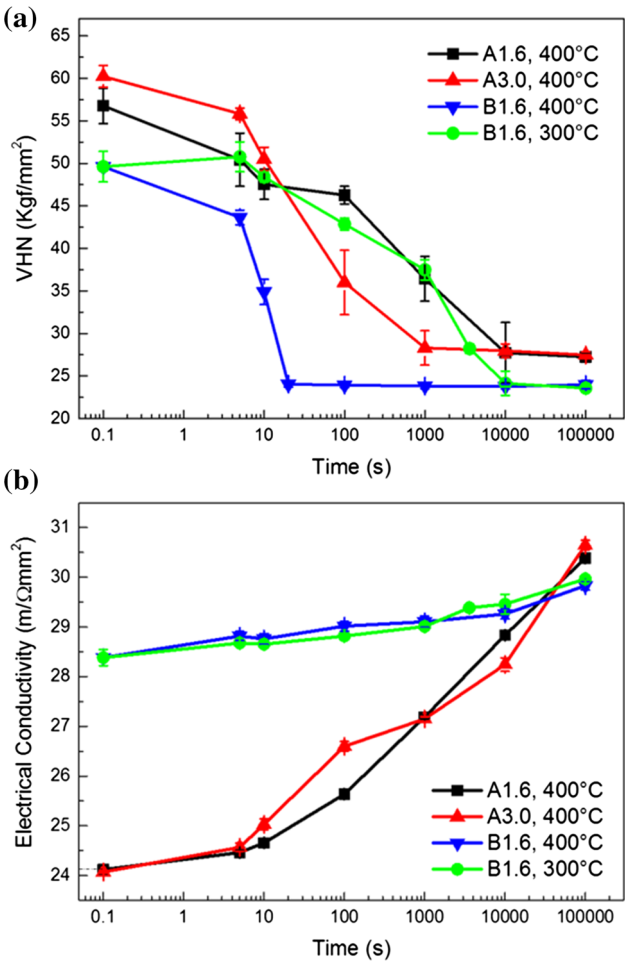

Fig. 2 Hardness and electrical conductivity variation of the samples during isothermal annealing at different temperatures **a** hardness and **b** electrical conductivity (Color figure online)

Recrystallization without concurrent precipitation

Based on the hardness evolution curve in Fig. 2a, a sample of B1.6 was annealed at 300 °C for 100 s, where no significant recrystallization was yet observed, as can be seen from both Figs. 2a and 3a. Since precipitation is very week, almost negligible (cf. Fig. 2b), for this variant, the slow recrystallization kinetics may either be due to low nucleation rate or due to low grain boundary mobility. In order to clarify this, two B1.6 samples were annealed at the higher temperature of 400 °C for 5 s in order to create more nuclei but resulting in only a small amount of recrystallized volume fraction. One of the samples was immediately quenched in water to freeze the microstructure after these 5 s, the EBSD map of which is shown in Fig. 3b where a lot of fine nuclei (nuclei that have already grown to large sizes) have appeared while the fraction recrystallized is still less than 5 %. The other sample was subsequently immersed into a salt bath preheated at 300 °C for another 100 s, with the additional annealing at 400 °C for 5 s, leading to complete recrystallization for this sample, as can be seen in Fig. 3c. It is worth noticing that, if the B1.6 sample was directly annealed at 400 °C, recrystallization completed within 20 s, as shown in Fig. 3d.

Recrystallization and precipitation occur concurrently

We now turn to other cases where strong concurrent precipitation is present during annealing, as indicated in Fig. 2b. After annealing at 400 °C for 100 s, recrystallization has started for the A1.6 sample, but the recrystallized fraction is very low (4 %), as evidenced in Fig. 4a. In fact, the recrystallized fraction has still only reached 14 % when increasing the annealing time to 200 s, see Fig. 4b. As was done for B1.6, two samples were annealed at a higher annealing temperature, in this case 450 °C, for 5 s. A fairly large number of small nuclei were observed after quenching one of the samples after this short annealing time; some examples are pointed out by black arrows in Fig. 4c. However, these nuclei did not help in reaching 100 % recrystallization for the other sample that was further annealed at 400 °C for another 100 s, as shown in Fig. 4d. Nonetheless, the recrystallized fraction (16 %) is comparable to the sample annealed at 400 °C for 200 s (see Fig. 4b).

Precipitation before recrystallization

It has been shown from Figs. 3 and 4 that recrystallization can be accelerated to different extents by performing a short time additional annealing at a higher temperature. For all the cases in Figs. 3 and 4, there is limited number of

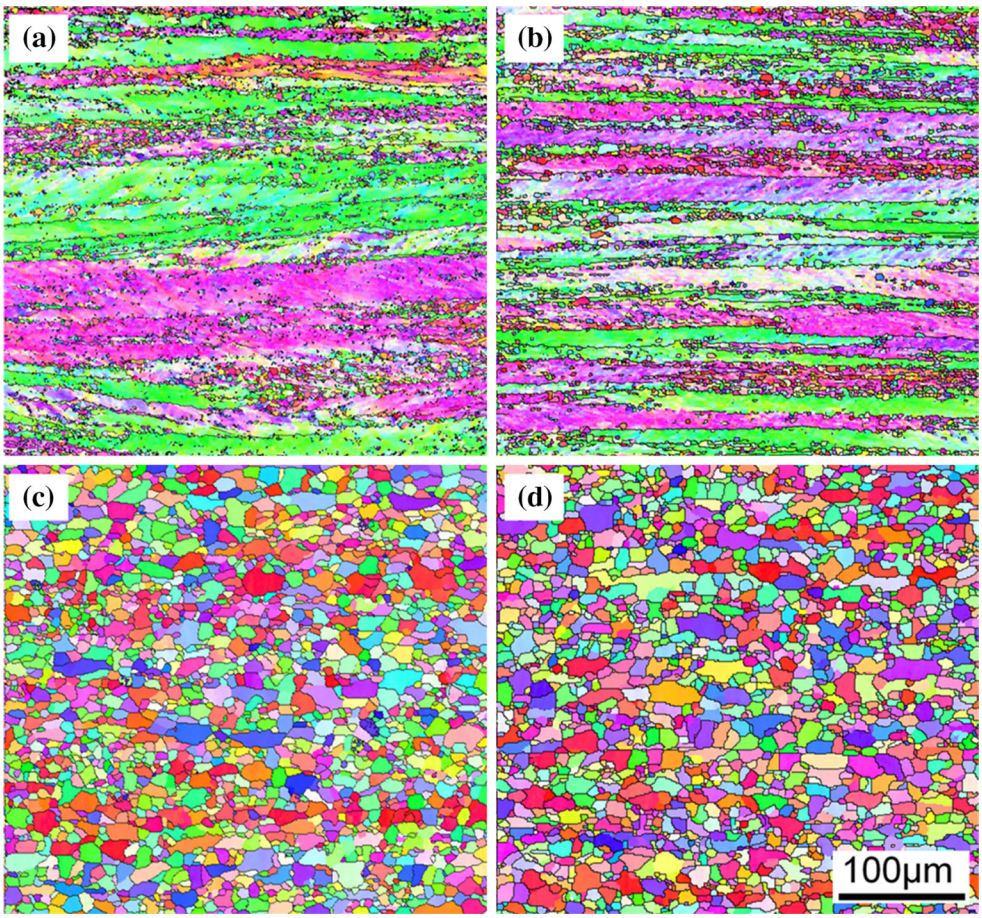

Fig. 3 EBSD maps showing the microstructures of B1.6 samples annealed at different conditions **a** $T = 300$ °C@100 s; **b** $T = 400$ °C@5 s; **c** $T = 400$ °C@5 s + 300 °C@100 s; **d** $T = 400$ °C@20 s (Color figure online)

dispersoids before annealing. There are other cases where most of the (sub)grain boundaries are occupied by dispersoids, which pins the migration of (sub)grain boundaries during subsequent annealing. One example is the A3.0 sample that has been heated at 50 °C/h to 300 °C and held at this temperature for 10^4 s, as shown in Fig. 5a. The dispersoids at (sub)grain boundaries will definitely suppress nucleation if one assumes that abnormal subgrain growth is the main "nucleation" mechanism during static recrystallization. Actually, recrystallization did not initiate even when the sample was further annealed at 300 °C until 10^5 s (see Fig. 5b). An interesting question to ask here is what will happen if we suddenly increase the annealing temperature for samples where (sub)grain boundaries initially are strongly pinned by dispersoids.

The samples of A3.0 heated at 50 °C/h to 300 °C and held for 10^4 s, where dispersoids are abundantly present at most of the (sub)grain boundaries (see Fig. 5a), were further annealed at 500 °C for 5 s. An almost fully recrystallized state was reached, with only a few non-recrystallized regions left as pointed out by black arrows in Fig. 6a. The recrystallized grains are clearly larger and more elongated along the RD as compared to the case of direct annealing in a salt bath at 500 °C for 5 s as shown in Fig. 6b. The average grain sizes were 31 and 19 μm for the samples after a two-step annealing and single-step annealing at 500 °C for 5 s, respectively.

Discussion

It is well known that decreased grain boundary mobility and slow nucleation rate, together with large amount of fine dispersoids jointly lead to slow recrystallization kinetics during annealing at low temperatures of supersaturated AA3xxx alloys. In order to identify the main mechanism behind the slow recrystallization for each of the conditions presented in "Results" section, a careful discussion is presented below with respect to the key aspects associated with sluggish recrystallization, i.e. incubation time, solute drag, and Zener drag. Possible ways to address these aspects in numerical modelling of sluggish recrystallization are also suggested.

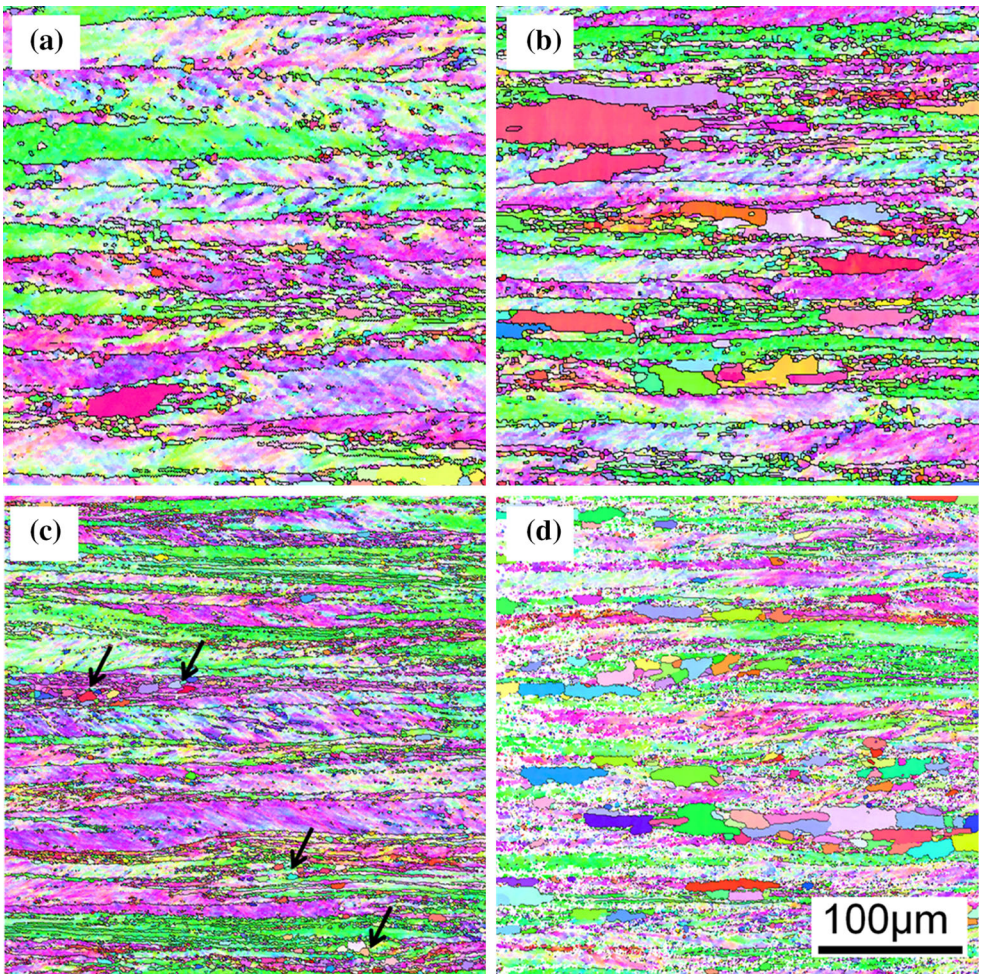

Fig. 4 EBSD maps showing the microstructures of A1.6 samples annealed at different conditions **a** $T = 400$ °C@100 s; **b** $T = 400$ °C@200 s; **c** $T = 450$ °C@5 s; **d** $T = 450$ °C@5 s + 400 °C@100 s (Color figure online)

The migration of low-angle (LAGB) and high-angle grain boundaries (HAGB), which both involve thermally activated jumps of atoms across the grain boundary, plays a central role during the annealing of cold-deformed metals. LAGB migration takes place during recovery and during the nucleation of recrystallization, while migration of HAGBs occurs both during and after primary recrystallization [1]. The mobility of HAGB (M_{pure}) follows an Arrhenius-type relation with temperature

$$M_{\text{pure}} = M_0 \exp\left(-\frac{Q}{RT}\right), \tag{1}$$

where M_0 is a pre-exponential factor, Q the apparent activation energy, R the gas constant, and T is the temperature. The mechanisms of LAGB migration are much less understood, but it is generally accepted that [1] (1) LAGB migrate at a rate consistent with (1); (2) LAGB migration is controlled by bulk diffusion processes; and (3) the boundary mobility increases with crystallographic misorientation.

Solute elements have an enormous effect on boundary migration and very small amounts of impurity may reduce the mobility by several orders of magnitude [1, 21–25]. In the current case, the mobility is mainly determined by the different Mn concentrations (X_{Mn}):

$$M = \left(\frac{1}{M_{\text{pure}}} + \alpha_{\text{drag}} X_{\text{Mn}}\right)^{-1}. \tag{2}$$

The drag effect from fine dispersoids on (sub)grain boundary migration (migration velocity V) is usually considered through the (sub)grain boundary mobility M and effective driving pressure P_{Eff}, as can be seen in (3). If we assume that nucleation occurs through the growth of certain subgrains with size and/or orientation advantage [26], in the early stage of growth, the pinning pressure (P_Z), along with the capillarity term from Gibbs–Thomson relationship (P_C), opposes the driving pressure (P) from stored energy which always decreases during annealing [1, 27].

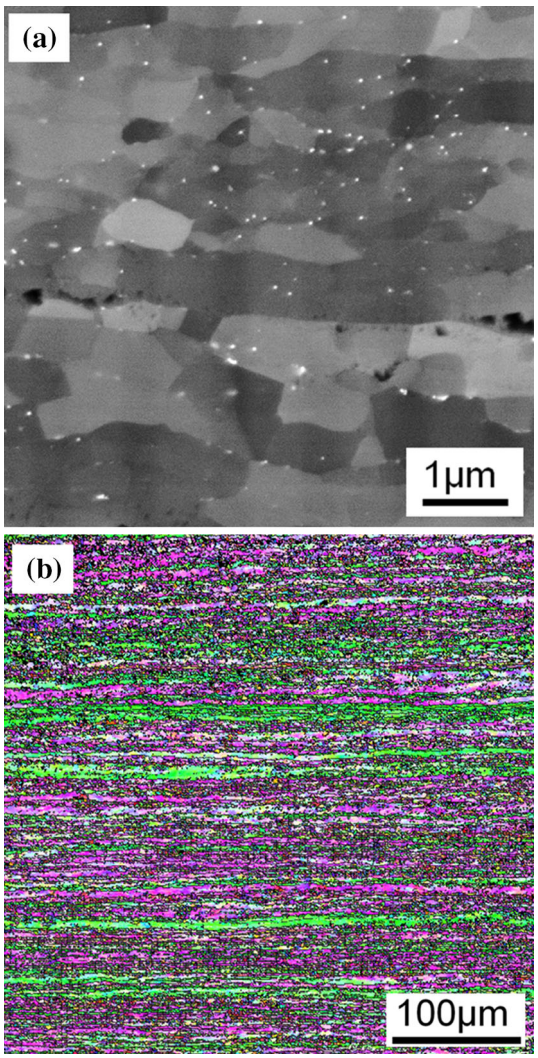

Fig. 5 The microstructure of A3.0 samples after annealing at different conditions **a** BSE image showing the fine dispersoids located at (sub)grain boundaries, the sample was heated at 50 °C/h to 300 °C and kept at this temperature for 10^4 s; **b** EBSD map showing the non-recrystallized microstructure, the sample was heated at 50 °C/h to 300 °C and kept for 10^5 s (Color figure online)

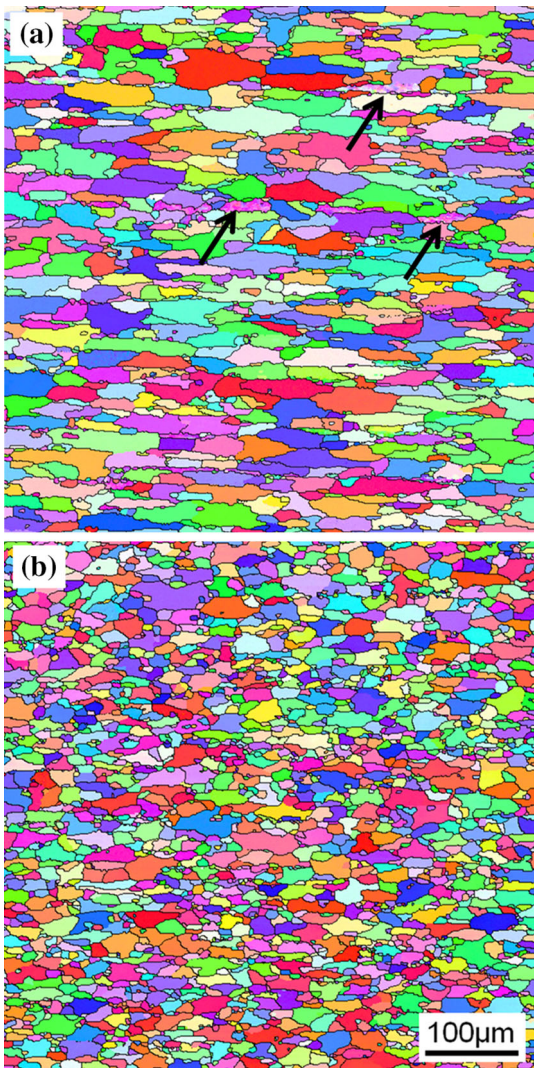

Fig. 6 The microstructures of A3.0 samples annealed at different conditions **a** EBSD map of A3.0 heated at 50 °C/h to 300 °C for 10^4 s and then annealed at 500 °C for 5 s; **b** EBSD map of A3.0 sample isothermally annealed at 500 °C for 5 s (Color figure online)

$$V = MP_{Eff} = M(P - P_C - P_Z), \tag{3}$$

where P_Z (Eq. 4) is dependent on subgrain boundary energy (γ), volume fraction (f), and average size (r) of the particles and P_C (Eq. 5) is related to both the subgrain boundary energy (γ) and the subgrain size (R):

$$P_Z = \frac{3\gamma f}{2r} \tag{4}$$

$$P_C = \frac{2\gamma}{R}. \tag{5}$$

Similar analysis also holds for nucleation through subgrain bulging into the neighbouring grain at grain boundaries, where the subgrain size in (5) should be replaced by the critical nucleus size, and only the HAGB energy is involved in (4) and (5). Equation (3) is most frequently used for HAGB migration, but subgrain boundaries can also be assumed to migrate according to this equation, except that the HAGB energy and mobility should be replaced by those valid for LAGB [1, 14, 28, 29]. Both quantities in general are significantly lower for LAGBs than for random HAGBs, and in particular the boundary energy depends on the boundary misorientation according to the Read–Shockley relationship [1] (i.e. increasing with increasing misorientation). For nucleation through subgrain growth to occur, it has, at the early stage of growth, to overcome the combined retarding effect of the capillarity term and a possible Zener pinning pressure, and the boundary migration velocity should be $V > 0$. It is worth

noticing that different Zener drag expressions have been developed, depending on the shape [30], location [31] and size distribution [32] of dispersoids, as well as the grain size [33], as compared to randomly distributed dispersoids. It should be mentioned that all these expressions are temperature independent, i.e. they predict the same Zener drag even if there is a sudden change of annealing temperature, as long as the size and volume fraction of the particles are unchanged (no dissolution or coarsening of particles). Moreover, although formally and quantitatively different, in most cases the magnitude of the Zener pressure is not significantly altered using these more refined expressions. In the present work, focusing on a qualitative analysis, Eq. (4) is therefore still used, as basis for the detailed discussion which follows below.

Incubation time

The B1.6 samples possess limited pre-existing dispersoids, and concurrent precipitation during annealing is also fairly weak (see Fig. 2b); for the purpose of simplification, we can thus assume that P_Z in (3) is negligible. It is clear from (1) that the mobility of grain boundary decreases with decreasing temperature. So the sluggish recrystallization for this variant at 300 °C should be most likely related to low grain boundary mobility or low nucleation rate. It is noted that with an initial heating at 400 °C for 5 s, a large number of recrystallized grains is produced, with a number density of $5.9 \times 10^3/\text{mm}^2$ (from Fig. 3b), and a fully recrystallized state can be reached during subsequent annealing at 300 °C within 100 s (see Fig. 3c). This observation indicates that the sluggish recrystallization kinetics of the B1.6 sample annealed at 300 °C cannot be attributed to the low mobility of HAGB grain boundaries. The sluggish recrystallization for B1.6 at this temperature, on the other hand, is due to weak nucleation (number density of recrystallized grains is only $\sim 1.3 \times 10^3/\text{mm}^2$ after 100 s from Fig. 3a), which in this case most probably is because the subgrain growth by LAGB migration is slow which limits the creation of successful nuclei, see Eq. (3). It is believed that the onset of recrystallization is controlled by the conversion of the dislocation arrangement into a subgrain structure, which would then provide a mobile grain boundary to allow a nucleus to grow [13], which corresponds to the incubation time for the onset of recrystallization. The short time annealing at 400 °C serves as a procedure to decrease the incubation time by accelerating the dislocation arrangement and subgrain growth, which actually yields more recrystallized grains (the number density increased from $5.9 \times 10^3/\text{mm}^2$ in Fig. 3b to $1.4 \times 10^4/\text{mm}^2$ in Fig. 3c) during the second step annealing at 300 °C. Without this acceleration, the second annealing step at 300 °C for 100 s gives rise no more than $\sim 1.3 \times 10^3/\text{mm}^2$ of new grains, which is the number density obtained when the sample was directly annealed at 300 °C for 100 s, as shown in Fig. 3a. The sluggish recrystallization for this kind of behaviour can thus be accounted for by numerical models [13, 14] through the introduction of an incubation time. Decreasing the grain boundary mobility in the model could possibly also fit the softening kinetics at the beginning of recrystallization, but it will definitely fail to predict the kinetics at later stages (from 1000 to 10000 s for B1.6) when growth of nuclei is dominating. It should be noted that our assumption that LAGB mobility follows (1) might be acceptable for a qualitative discussion, but this assumption is most likely too restrictive for quantitative modelling, since detailed experimental work has shown that LAGB and HAGB mobilities can have a different temperature dependency [34].

Moreover, as listed in Table 2, the incubation time varies with annealing temperature, cold deformation, and solute level. Recrystallization started at different times for B1.6 annealed at 300 and 400 °C, where in the latter case at 400 °C the incubation time is less than 5 s (see Fig. 3b) while ~100 s at 300 °C (Fig. 3a). The shorter incubation time at 400 °C for B1.6 is mainly due to subgrains growing faster due to their increased boundary mobility (negligible pinning force from fine dispersoids for both cases), which leads to a rapidly decreasing P_C, i.e. subgrains grow faster and more numerously overcome the critical size for nucleation and become viable recrystallization nuclei, and which further favours their growth. Increasing the cold deformation also promotes shorter incubation times. As can be seen from Fig. 2a, recrystallization initiated at about 5 s for A3.0, while the incubation time was about 100 s for A1.6. If we neglect the subtle variation of microchemistry and subgrain size between these two samples, the increased driving pressure (P) in Eq. (3) is responsible for the shorter incubation time of A3.0. The different incubation times ($t_{A1.6} > t_{B1.6}$) during annealing of A1.6 and B1.6 at 400 °C can be attributed to the different solute levels of Mn. The significant supersaturation of Mn in A1.6 (see Fig. 2b) diffuses to create fine dispersoids at (sub)grain boundaries and thus providing a substantial retarding force P_Z, causing a reduced P_{Eff} in Eq. (3). Also Mn in solid solution will

Table 2 The approximate incubation time for different isothermal annealing conditions

Condition	Incubation time (s)
A1.6, annealed at 400 °C	~100
A3.0, annealed at 400 °C	~5
B1.6, annealed at 300 °C	~100
B1.6, annealed at 400 °C	~5

retard the recovery process through a solute drag effect on the subgrain boundaries. Both factors act to delay the formation of critically sized subgrains as potential nuclei [1].

Solute drag and Zener pinning

Slow recrystallization kinetics was also obtained for samples of A1.6 annealed at 400 °C, as shown in Fig. 2a. Even though it was annealed at a temperature 100 °C higher than B1.6 (300 °C), similar recrystallization kinetics was still observed for these two cases (Fig. 2a). Since the applied strain is the same, and the grain boundary mobility according to Eq. (1) (considering just the temperature effect) in principle is higher for the A1.6 sample, it should result in faster recrystallization for A1.6, if the microchemistries of A1.6 and B1.6 are the same. However, at least two factors are involved which may help in understanding the sluggish recrystallization behaviour of the A1.6 sample annealed at 400 °C. Firstly, the microchemistry is not the same as the solute level of Mn in A1.6 is much higher than that of B1.6. If we assume that other alloying elements affect both A1.6 and B1.6 equally, we have according to Eq. (2) a lower boundary mobility for the recrystallized grains of A1.6, due to its higher solute level (X_{Mn}). Secondly, as shown in Fig. 2b, the electrical conductivity increased by 1.5 m/Ωmm^2 during annealing for 100 s at 400 °C, which is an indication of significant *concurrent* precipitation, and P_Z is no longer negligible. The drag effect from fine dispersoids on grain boundary migration (migration velocity V) expressed through the drag force P_Z thus reduces the net driving pressure according to Eq. (3).

From the above analysis, it is not surprising that A1.6 recrystallized much more slowly than B1.6 (see the black and blue lines in Fig. 2a) at 400 °C. Additional two-step annealing experiments as illustrated in Fig. 1b were also conducted to further investigate the sluggish recrystallization behaviour for the A1.6 sample. The short time (5 s) annealing at 450 °C indeed produced a noticeable number of nuclei in the sample of A1.6, as shown in Fig. 4c. It should be noted that these nuclei/grains are more or less randomly distributed, with average size of 5 μm and number density of $\sim 1.7 \times 10^3$/mm^2. When the sample was subsequently annealed at 400 °C for another 100 s, ~16 % of the material was recrystallized as compared to ~4 % for the sample subjected to the single-step annealing at 400 °C for 100 s. If we neglect the microchemistry changes in terms of solute level and second-phase particle structures during the short annealing time at 450 °C, it can be assumed that the solute drag and Zener drag from dispersoids for the two samples presented in Fig. 4a, d are similar, and the main difference is the amount of nuclei (recrystallized grains) created during the first high temperature annealing step. After the second annealing step at 400 °C for 100 s (see Fig. 4d), the number density of recrystallized grains decreased to $\sim 1.4 \times 10^3$/mm^2, while the average grain size of recrystallized grains of the partially recrystallized grain structure reached 16 μm. A similar decrease in number density of recrystallized grains was also observed when increasing the annealing time from 100 s (0.8×10^3/mm^2, Fig. 4a) to 200 s (0.5×10^3/mm^2, Fig. 4b) during isothermal annealing at 400 °C. Even though the available data may not be statistically reliable, it is still reasonable to assume that some of the recrystallized grains formed at early recrystallization stages, when the amount of concurrently precipitated dispersoids was still limited, did not grow further, possibly due to the increased pinning pressure from continuously precipitated fine dispersoids at later stages. The influence of this latter pinning force on the recrystallized grain boundaries was regarded as a negligible effect on the recrystallization kinetics in the model and modelling work presented in [12], and it is possibly also the reason why a steeper than experimental recrystallization kinetics curve was predicted when annealing a hot-rolled ($\varepsilon = 0.69$) AA3103 at 375 °C in their case. The reason why still a significant fraction of the recrystallized grains formed after annealing at 450 °C for 5 s can continue to grow at the lower annealing temperature is most probably due to fluctuations in size and, thus in P_C.

Temperature-dependent effective retarding force

When substantial precipitation occurs before the onset of recrystallization at low annealing temperature, as shown in Fig. 5a for the A3.0 sample, recrystallization can be totally suppressed (see Fig. 5b) if the sample is kept at this low temperature. In this case, most of the subgrains are pinned by fine dispersoids and thus not able to grow to overcome the combined opposing effect of the capillarity force and Zener drag ($P_{Eff} = 0$ in Eq. (3)). However, if this sample is further annealed for a short time at a higher temperature (in this case, 5 s at 500 °C), nucleation can still be activated and recrystallization has almost completed within this short time of annealing, as shown in Fig. 6a. The question is how can we explain the fact that recrystallization can be reactivated (not to mention almost fully recrystallized) when a sample initially pinned by dispersoids (see Fig. 5a) is further annealed at 500 °C for 5 s. One may argue that the effective driving force P_{Eff} is just very small (at least for some of the subgrains), but still positive after the first annealing step (heating at 50 °C/h to 300 °C and kept for 10^4 s). The sudden increase of annealing temperature significantly increases the subgrain boundary mobility M and the accompanying subgrain boundary migration velocity,

and thus provides a significant amount of subgrains (within a reasonable time) to overcome the critical size for growth ($P_{Eff} > 0$) in (5), i.e. successful nucleation. However, as P_{Eff} in principle should decrease when switching to a higher annealing temperature, as discussed further below, the net effect of an increased mobility M and decreased P_{Eff} on subgrain boundary migration V is not obvious.

It is evident from Fig. 5a, i.e. when the sample was heated at 50 °C/h to 300 °C and kept at this temperature for 10^4 s, that most of the grain/subgrain boundaries are pinned by precipitated fine dispersoids. Actually, if some of them are able to move slowly, one should be able to observe some dispersoids behind the moving boundaries of these subgrains, which does not seem to be the case according to Fig. 5a. It is thus reasonable to consider $P_{Eff} = 0$ before the annealing at 500 °C for 5 s. In order to provide $P_{Eff} > 0$, we should either have a larger driving pressure (P) or decreased opposing pressure (through P_C and/or P_Z), regardless of the subgrain mobility. When switching to higher annealing temperatures, driving pressure P obviously cannot increase, and the subgrains are not able to grow since their boundaries are pinned by fine dispersoids, i.e. a stabilized subgrain structure with a fixed average subgrain size, which leaves P_C unchanged. Also, it is not expected that the fine dispersoids can grow or dissolve significantly within only 5 s at 500 °C. Actually, as shown in Fig. 7b, fine dispersoids can still clearly be observed both within the recrystallized grains as well as at the growing front of the recrystallizing grains. In the present study, the A3.0 sample was previously annealed at 300 °C for 10^4 s which expectedly should have significantly reduced the dislocation density in the deformed structure, at the same time, the average size of the precipitates after this long annealing time is quite large (~50 nm), presumably large enough to avoid being dissolved in 5 s at 500 °C. For the samples of A series, it has been shown that the EC keeps increasing either during isothermal annealing at 500 °C [7] or non-isothermal annealing at 50 °C/h up to 500 °C [9], i.e. there are no indications of dissolution of particles (decreasing of EC) after annealing for 5 s at 500 °C. Careful measurement from BSE micrographs before (see Fig. 5a) and after short time high temperature annealing (see Fig. 7) reveals that the average size of the precipitates are similar (~50 nm), which is obviously above the detection limit of the BSE detector (~10 nm) and implies there is no coarsening either. Strictly speaking, since static recovery does not need an incubation time, annealing at a higher temperature for a short time will actually contribute to a somewhat higher subgrain boundary energy (γ) due to an increased boundary misorientation caused by recovery [1]. Recovery should thus in principle lead to a decreased P and increased P_Z (according to (4)) and P_C (according to 5), all of which provide a reduced P_{Eff} which should make the formation of recrystallization nuclei even more difficult. This is clearly not consistent with our experimental observations, which show that the short time annealing at 500 °C actually lead to almost full recrystallization. One possible explanation is related to the effect of solutes, as assumed in the present paper, the main influence of solutes is mostly considered to be on the grain boundary mobility [1]. But solutes may have a strong influence on opposing the recovery processes (in terms of subgrain growth) and thus affect the driving force for recrystallization, i.e. another retarding pressure due to solute drag (P_{sol}) should be added in (3) [1, 35]. The fact that adding the solute drag as a retarding force helps give a more accurate prediction of recrystallization process

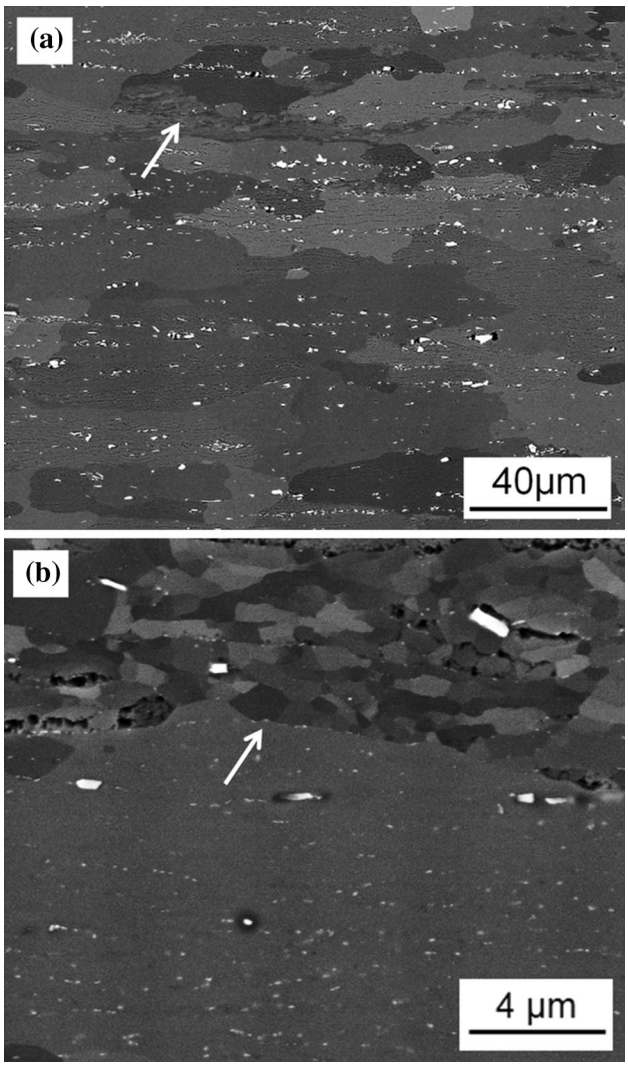

Fig. 7 BSE images showing the microstructures of A3.0 samples heated at 50 °C/h to 300 °C for 10^4 s and then annealed at 500 °C for 5 s **a** An overview of the microstructure, the *white arrow* showing the small fraction of non-recrystallized area (see Fig. 6a); **b** High-magnification image showing GB being dragged by dispersoids as pointed out by *white arrow*

that was documented in [36]. The solute drag, however, becomes less effective at high temperatures [1, 22], which then explains why the sudden increase of temperature can lead to $P_{Eff} > 0$. It may also be speculated that the actual Zener drag (P_Z) in (3) is decreased at higher temperatures, which indicates that the classical expression for P_Z (Eq. (4)), not explicitly dependent on temperature, should be modified to account for such a decreased P_Z at higher annealing temperatures. Once the Zener drag becomes less effective (lower value of P_Z), the subgrains start growing ($V > 0$), P_C also decreases ($\sim 1/R$), and nucleation can be activated. A quantitative calculation of the effective driving force based on the experimental results was discussed in [8], where it was found that the calculated driving force was still larger than the opposing forces at sluggish recrystallization conditions (low annealing temperatures). This also suggests that the Zener pinning force might be temperature dependent and it is larger than the calculated value according to (4) at low annealing temperatures.

Clues for coupled recrystallization and precipitation models

From the above analysis, it is obvious that numerical models that couple precipitation and recrystallization are needed for giving adequate predictions of the microstructure evolution during sluggish recrystallization. Our experimental results provide valuable information for numerical modelling of sluggish recrystallization of high stacking fault energy particle-containing materials, which can be summarized as follows:

1. In conditions for sluggish recrystallization, a distinct incubation time before the onset of recrystallization is commonly observed. This implies that site-saturated nucleation (i.e. a certain number density of nuclei all start to grow at $t = 0$), a commonly used assumption in many recrystallization models [1, 37], is clearly not consistent with reality for these conditions.
2. For the same material, the recrystallization kinetics can change significantly if the microchemistry in terms of solute level and second-phase particle structure is altered. A fully adequate model should thus be able to consider the microchemistry evolution during the annealing process.
3. Numerical models with physically based nucleation laws designed for non-isothermal or variable conditions should be able to consider a time dependent and possibly also a temperature-dependent effective retarding force from solute and/or particles, a solute drag-dependent grain boundary mobility, cell structure evolution, as well as suppressed nucleation by concurrent precipitation at (sub)grain boundaries.

Conclusions

In this study, the sluggish recrystallization behaviour of a cold-rolled Al–Mn–Fe–Si alloy has been investigated. Experiments were conducted at carefully chosen thermo-mechanical conditions such that sluggish recrystallization in three different scenarios can be analysed, i.e. (i) recrystallization without precipitation; (ii) recrystallization concurrently with precipitation; and (iii) precipitation before the onset of recrystallization. Meanwhile, some simple complementary experiments were also performed to make comparisons with the above-mentioned ones. Distinctly different recrystallization behaviours have been observed when the microchemistry of the materials and the annealing conditions are changed. The following conclusions can be drawn:

1. In conditions for sluggish recrystallization, a distinct incubation time before the onset of recrystallization is commonly observed. The incubation time is found to decrease with annealing temperature and cold deformation, and to increase with initial solute level. This implies that the site-saturated nucleation assumption often used when modelling recrystallization in aluminium alloys is not appropriate for these conditions.
2. Higher solute levels lead to slower recovery, lower (sub)grain boundary mobility, and higher potential for concurrent precipitation, all of which combine together to produce a sluggish recrystallization behaviour.
3. When precipitation occurs concurrently with recrystallization, it not only retards the grain boundary migration of recrystallized grains but also significantly decreases the nucleation rate.
4. Strongly pinned subgrains can be activated for further growth at higher annealing temperatures, while the growth of successful nuclei can still be suppressed by further concurrent precipitation at lower annealing temperatures.
5. Qualitative analysis of the microstructure evolution after sudden increase of annealing temperature suggests that the effective retarding force from solute and/or particles decreases at higher temperatures, which should be considered for analysing and modelling of sluggish recrystallization.

Acknowledgements This research work has been supported by the KMB project (193179/I40) in Norway. The financial support by the Research Council of Norway and the industrial partners, Hydro

Aluminium and Sapa Technology is gratefully acknowledged. KH and REL acknowledge the financial support from PX group.

References

1. Humphreys FJ, Hatherly M (2004) Recrystallization and related annealing phenomena, 2nd edn. Elsevier, Oxford
2. Li YJ, Arnberg L (2003) Quantitative study in the precipitation behavior of dispersoids in DC-cast AA3003 alloy during heating and homogenization. Acta Mater 51:3415–3428
3. Li YJ, Arnberg L (2003) Evolution of eutectic intermetallic particles in DC-cast AA3003 alloy during heating and homogenization. Mater Sci Eng A 347:130–135
4. Somerday M, Humphreys FJ (2003) Recrystallization behavior of supersaturated Al-Mn alloys. Mater Sci Technol 19:20–29
5. Liu WC, Morris JG (2005) Evolution of recrystallization and recrystallization texture in continuous-cast AA 3015 aluminum. Metall Mater Trans A 36:2829–2848
6. Sjølstad K, Engler O, Tangen S, Marthinsen K, Nes E (2002) Recrystallization textures and the evolution of the P-orientation as a function of precipitation in an AA3103 alloy. Mater Sci Forum 408–412:1471–1476
7. Huang K, Wang N, Li YJ, Marthinsen K (2014) The influence of microchemistry on the softening behaviour of two cold-rolled Al-Mn-Fe-Si alloys. Mater Sci Eng A 601:86–96
8. Marthinsen K, Wang N, Huang K (2014) Modelling microstructure and properties during annealing of cold rolled Al-Mn-Fe-Si-alloys with different microchemistries. Mater Sci Forum 783–786:57–62
9. Huang K, Engler O, Li YJ, Marthinsen K (2014) Evolution in microstructure and properties during non-isothermal annealing of a cold-rolled Al-Mn-Fe-Si alloy with different microchemistry states. Mater Sci Eng A 628(2015):216–229
10. Jones MJ, Humphreys FJ (2003) Interaction of recrystallization and precipitation: the effect of Al_3Sc on the recrystallization behaviour of deformed aluminium. Acta Mater 51:2149–2159
11. Rehamn MK, Zurob HS (2013) A novel approach to model static recrystallization of austenite during hot rolling of Nb microalloyed steel. Part I: Precipitate-free case. Metall Mater Trans A 44:1862–1871
12. Miroux A, Lok ZJ, Van der Zwaag S (2004) Recrystallisation and concurrent precipitation in hot rolled AA3103. Mater Sci Forum 467–470:393–398
13. Schäfer C, Mohles V, Gottstein G (2011) Modeling of non-isothermal annealing: interaction of recrystallization, recovery, and precipitation. Acta Mater 59:6574–6587
14. Zurob HS, Bréchet Y, Dunlop J (2006) Quantitative criterion for recrystallization nucleation in single-phase alloys: prediction of critical strains and incubation times. Acta Mater 54:3983–3990
15. Lefevre-Schlick F, Brechet Y, Zurob HS, Purdy G, Embury D (2009) On the activation of recrystallization nucleation site in Cu and Fe. Mater Sci Eng A 502(2009):70–78
16. Birol Y (2008) Impact of homogenization on recrystallization of a supersaturated Al-Mn alloy. Scr Mater 60:5–8
17. Engler O, Liu Z, Kuhnke K (2013) Impact of homogenization on particles in the Al-Mg-Mn alloy AA 5454—experiment and simulation. J Alloys Compd 56:0111–0122
18. Huang K, Zhao Q, Li Y, Marthinsen K (2015) Two-stage annealing of a cold-rolled Al-Mn-Fe-Si alloy with different microchemistry states. J Mater Process Technol 221:87–99
19. Huang K, Li Y, Marthinsen K (2014) Isothermal annealing of a cold-rolled Al-Mn-Fe-Si alloy with different microchemistry states. Trans Nonferrous Met Soc China 24:3840–3847
20. Huang K, Li Y, Marthinsen K (2015) Effect of heterogeneously distributed dispersoids on the recrystallization behavior of Al-Mn-Fe-Si alloys. Mater Character 10:292–297
21. Cahn JW (1962) The impurity-drag effect in grain boundary motion. Acta Metall 10:789–798
22. Lücke K, Stüwe H-P (1963) On the theory of grain boundary motion. In: Himmel L (ed) Recovery and recystallization of metals. Wiley, New York, pp 171–210
23. Lücke K, Stüwe HP (1971) On the theory of impurity controlled grain boundary motion. Acta Metall 19:1087–1099
24. Hersent E, Marthinsen K, Nes E (2013) The effect of solute atoms on grain boundary migration: a solute pinning approach. Metall Mater Trans A 44A:3364–3375
25. Hersent E, Marthinsen K, Nes E (2014) On the effect of atoms in solid solution on grain growth kinetics. Metall Mater Trans A 45A:4882–4890
26. Huang Y, Humphreys FJ (2000) Subgrain growth and low angle boundary mobility in aluminium crystals of orientation $\{110\}\langle 001\rangle$. Acta Mater 48:2017–2030
27. Hallberg H, Svendsen B, Kayser T, Ristinmaa M (2014) Microstructure evolution during dynamic discontinuous recrystallization in particle-containing Cu. Comput Mater Sci 84:327–338
28. Sandstrom R (1977) Subgrain growth occurring by boundary migration. Acta Metall 25:905–911
29. Varma SK (1986) Effects of the amount of prior cold work and annealing temperature on subgrain growth in Al-0.2Mg alloy. Mater Sci Eng 82:19–22
30. Nes E, Ryum N, Hunderi O (1985) On the Zener drag. Acta Metall 33:11–22
31. Daaland O, Nes E (1996) Recrystallization texture development in commercial Al-Mn-Mg alloys. Acta Mater 44:1413–1435
32. Eivani A, Valipour S, Ahmed H, Zhou J, Duszczyk J (2011) Effect of the size distribution of nanoscale dispersed particles on the zener drag pressure. Metall Mater Trans A 42A:1109–1116
33. Bréchet Y, Militzer M (2005) A note on grain size dependent pinning. Scr Mater 52:1299–1303
34. Winning M, Rollett AD, Gottstein G, Srolovitz DJ, Lim A, Shvindlerman LS (2010) Mobility of low-angle grain boundaries in pure metals. Philos Mag 90:3107–3128
35. Cram DG, Fang XY, Zurob HS, Bréchet YJM, Hutchinson CR (2012) The effect of solute on discontinuous dynamic recrystallization. Acta Mater 60:6390–6404
36. Bäcke L (2010) Modeling the effect of solute drag on recovery and recrystallization during hot deformation of Nb microalloyed steels. ISIJ Int 50:239–247
37. Vatne HE, Furu T, Ørsund R, Nes E (1996) Modelling recrystallization after hot deformation of aluminium. Acta Mater 44:4463–4473